12-28-2008

Photopolymerization-Induced Crystallization and Phase Separation in Poly(Ethylene Oxide)/Triacrylate Blends

Soo Jeoung Park

Thein Kyu
University of Akron Main Campus, tkyu@uakron.edu

Photopolymerization-induced crystallization and phase separation in poly(ethylene oxide)/triacrylate blends

Soo Jeoung Park and Thein Kyu[a)]
Department of Polymer Engineering, University of Akron, Akron, Ohio 44325, USA

(Received 23 September 2008; accepted 12 November 2008; published online 22 December 2008)

The present article describes experimental and theoretical investigations of miscibility and crystallization behavior of blends of poly(ethylene oxide) (PEO) and triacrylate monomer (TA) using differential scanning calorimetry and optical microscopy. The PEO/TA blends manifested a single T_g varying systematically with composition suggestive of a miscible character in their amorphous states. Moreover, there occurs melting point depression of PEO crystals with increasing TA. A phase diagram was subsequently established that exhibited a solid+liquid coexistence region bound by the liquidus and solidus lines, followed by an upper critical solution temperature (UCST) at a lower temperature. The emerging phase morphology was investigated to verify the coexistence regions. Upon photopolymerization in the isotropic melt above the melting point depression curve, both the UCST and the melting temperatures move upward and eventually surpass the reaction temperature, resulting in phase separation as well as crystallization of PEO driven by the changing supercooling, i.e., the thermodynamic driving force. Of particular interest is the interplay between photopolymerization-induced phase separation and crystallization, which eventually determines the final phase morphology of the PEO/TA blend such as crystalline lamellae, sheaf, or spherulites in isotropic liquid, phase separated domains, and viscous fingering liquids. © *2008 American Institute of Physics*. [DOI: 10.1063/1.3040279]

I. INTRODUCTION

Miscibility of polymer blends has been studied extensively, with most of the investigated systems representing mixtures of two amorphous polymers.[1–3] However, crystalline polymer blends have received very little attention as compared to fully amorphous systems due to complex crystallization habits and intricate crystalline morphology[4] displayed by either one or both constituents.[5–14] Moreover, the resulting phase separated domains and associated crystalline morphologies are nonequilibrium and nonlinear in nature. These dynamical pattern forming processes are primarily governed by the competition between liquid-liquid phase separation and solid-liquid phase transition (i.e., crystallization).[9–14] Recently, the complex interplay of the two nonequilibrium processes has prompted the experimental and theoretical investigations of the miscibility and crystallization behavior of crystalline polymer blends.[15–18] Moreover, when one of the constituents is a reactive monomer, polymerization-induced crystallization can occur in a manner dependent on the kinetic pathways across the phase diagrams.[19] Matkar and Kyu[20,21] and Matsuyama[22] have been some of the advocates to point out the usefulness of establishing thermodynamic phase diagrams because it offers practical guidance for analyzing the emerging crystal morphology as the system traverses across various coexistence regions.

In this paper, the miscibility and phase behavior of blends of poly(ethylene oxide) (PEO) and triacrylate monomer (TA) were investigated by means of differential scanning calorimetry (DSC) and polarized optical microscopy. The solid-liquid phase diagram was established both experimentally and theoretically based on the combined Flory–Huggins (FH) free energy for liquid-liquid demixing[3] and phase field free energy of crystallization.[20,23–26] To verify the predicted coexistence regions, the emerging phase morphologies of the crystalline PEO/amorphous TA blends were examined by thermal quenching into each coexistence region. Subsequently, photopolymerization was carried out in the isotropic melt, i.e., slightly above the melting point depression curve, which pushes up the coexistence curves to surpass the reaction temperature. Of particular importance is the interplay between photopolymerization-induced phase separation and crystallization, which eventually determines the final phase morphology of the PEO/TA blend such as crystal+liquid phase transition, liquid+liquid phase separation, and viscous fingering phenomena.

II. EXPERIMENTAL SECTION

PEO was purchased from Scientific Polymer Products, Inc. having a reported weight average molecular weight of M_w=66 000 with a polydispersity of 1.94. Trimethyolpropane TA having a weight average molecular weight (M_w) of 296.3 g/mol with a density of 1.1 g/ml was supplied by Aldrich Chemical Co.

Various concentrations of PEO were dissolved in TA monomer at an elevated temperature in a water bath maintained at 70 °C on a sample hot-plate. The melting transition temperatures of the PEO crystal in its TA blends were established using DSC (model Q-1000, TA Instruments). Various

[a)]Author to whom correspondence should be addressed. Electronic mail: tkyu@uakron.edu.

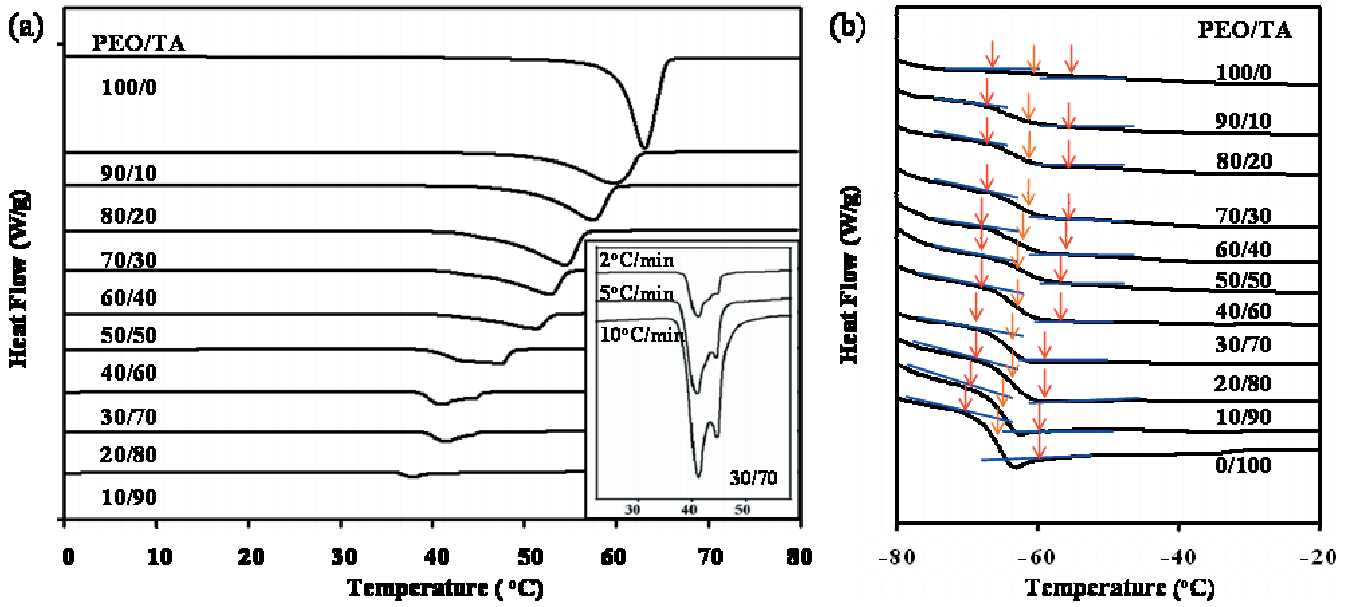

FIG. 1. (Color) (a) DSC thermograms of PEO/TA blends showing a depression of the melting peak of PEO with the addition of TA. The inset represents the enlarged dual melting peaks of PEO/TA 30/70 in various heating rates showing dual melting endotherms at low PEO contents. (b) DSC thermograms of PEO/TA blends showing a systematic shift of T_g's with PEO contents. The heating rate was 2 °C/min.

heating rates were carried out for all PEO/TA mixtures (e.g., 2, 5, and 10 °C/min). The endothermic peaks of the second heating cycle were regarded as the melting points, whereas the midpoint of the transition zone was taken as the glass transition (T_g) of the PEO/TA blends.

The phase morphology of the blends was examined using a polarized optical microscope (Olympus-BX60) equipped with a microscope hot-stage (TMS 93, Linkam). The isotropic melt PEO/TA blends were sandwiched between two optical glass slides and then heated to 80 °C to ensure reaching the steady melt state. To verify the predicted crystal+isotropic liquid and single-phase crystal regions, the emerging phase morphology was examined following isothermal quenching from 80 °C to various temperatures corresponding to various coexistence regions of the PEO/TA phase diagram.

Regarding photopolymerization, rose bengal photoinitiator[27] (1 wt % of reactive monomer) was used with the aid of *N*-phenyl glycine (coinitiator), *N*-vinyl pyrrolidone (solubilizing agent), and octanoic acid (surfactant).[28,29] The rose bengal ester possesses two broad absorptions in the regions of 350–440 and 450–560 nm having a high triplet quantum yield of 0.76.[27] The photocuring reaction was carried out for various PEO/TA mixtures by subjecting the samples (weighing 7 mg) to uniform ultraviolet illumination at 365 nm and 40 mW/cm^2 for 10 min at 70 °C. In the time-resolved optical microscopic studies, the photocurable PEO/TA/rose bengal samples were sandwiched between the glass slide and the cover glass after melting at 70 °C for 10 min. These sandwiched samples were exposed to green filtered light (at 532 nm) to trigger free radical photopolymerization of TA in the mixtures. The emerging microstructures were photographed using a digital camera (Canon, EOS 300D) as a function of reaction time, blend composition, and reaction temperatures under appropriate magnifications ranging from 50× to 500×.

III. RESULTS AND DISCUSSION

A. Miscibility characterization

Figure 1(a) exhibits the DSC thermograms of PEO/TA blends obtained at a heating rate of 2 °C/min. The melting transition of PEO was found to decrease with increasing TA content. The observed melting point depression of PEO with TA content is consistent with those reported for other miscible or partially miscible blends,[30,31] except that there appear dual melting peaks of PEO in the thermograms, especially at low PEO concentrations. Such dual peaks are discernible at the faster scans of 5 and 10 °C/min in the enlarged scale shown in the inset, which in turn confirm the reproducibility of these dual peaks at low PEO concentrations.

One of the criteria most commonly used for determining polymer blend miscibility of binary amorphous blends is to examine the variation in glass transition temperature as a function of composition. Figure 1(b) depicts the T_g of pure PEO and TA at −60.7 and −65.8 °C, respectively. The intermediate blends show a single T_g varying systematically with blend ratios, while their transition width remains comparable to those of the constituents. These observed behaviors of T_g and the melting point depression imply that the PEO/TA blends may be miscible in the amorphous state. This conjecture may be tested based on the analysis of the dependence of T_g on blend composition according to the classical Fox equation in what follows:[1,2]

$$\frac{1}{T_{g,\text{blend}}} = \frac{X_1}{T_{g,1}} + \frac{X_2}{T_{g,2}}, \tag{1}$$

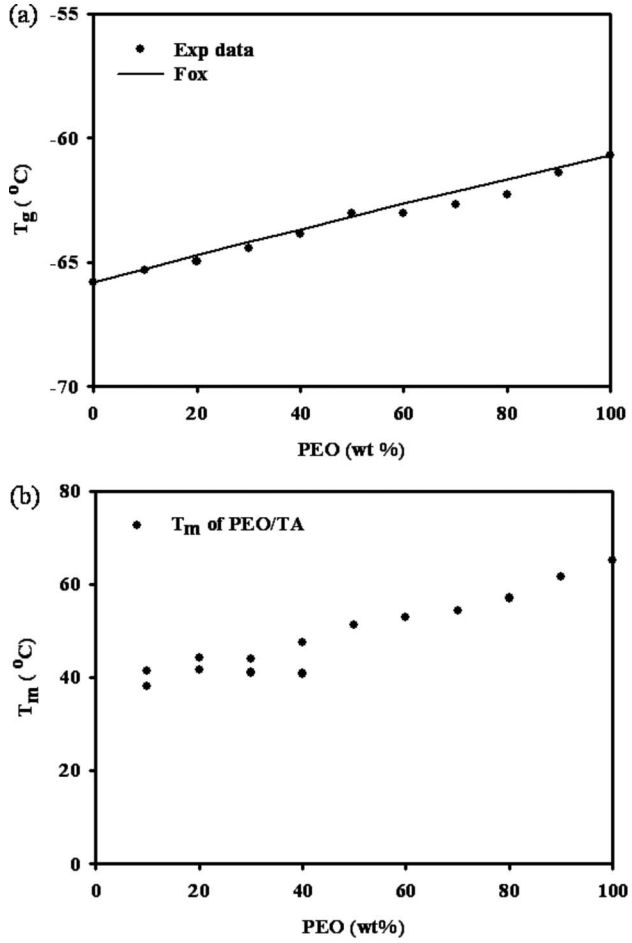

FIG. 2. Plots of (a) glass transition temperature with PEO concentrations in comparison with Fox equation implying amorphous-amorphous miscibility and (b) melting point depression of PEO. The negative departure may be a consequence of PEO crystals preventing complete miscibility in the amorphous phase at high PEO contents.

where subscripts 1 and 2 represent PEO and TA, respectively, with X_i being the weight fraction of component i. Figure 2(a) exhibits the observed T_g as a function of PEO content in comparison with the Fox equation, showing a reasonable fit except for higher PEO contents. This slight negative departure from the Fox prediction, if any, may be attributed to the crystallinity of PEO, which probably prevents the system from achieving complete miscibility.

Figure 2(b) shows the experimental melting points (T_m) of the PEO crystal in its blends with TA as a function of composition, as obtained by extrapolating the rate dependent T_m values to a zero heating rate. Although the T_m at the extrapolated zero heating rate may not truly represent equilibrium, it may be sufficient for describing the relative trends of the T_m values as a function of blend concentrations. It is worthy to note that the melting transition of PEO is lowered as the TA content increases. At low PEO compositions, there appear dual melting transitions, thereby complicating the assignment of these transitions. As demonstrated by Matkar and Kyu,[20] it is beneficial to establish phase diagrams in order to determine various coexistence regions involving isotropic melt (I), crystal+isotropic melt (Cr+I), and single-phase crystal (Cr) regions.

B. Phase diagrams

The phase diagram of PEO/TA is solved self-consistently in accordance with the theory of Matkar and Kyu.[20] In their model, the original assumption of the Flory diluent theory of crystalline polymer solutions, namely, the complete rejection of the polymeric solvent from the crystalline phase,[3] was removed by allowing the solvent to reside (or be trapped) within the crystalline phase.[11,12,20,21] Of particular importance is that their theory takes into consideration the interaction between the crystalline and amorphous phases in addition to the amorphous-amorphous interaction.[20,21] The free energy of a crystalline polymer blend was expressed in terms of a combination of FH free energy of liquid-liquid demixing,[3] phase field free energy of crystal solidification given by the Landau-type double well potential,[23–26] coupling free energy representing the interaction between the amorphous phase and the crystalline phase,[20,21]

$$f_{\text{overall}}(\psi,\phi) = f_{\text{mixing}} + \phi f_{\text{crystal}} + f_{\text{coupling}}. \tag{2}$$

The FH free energy of mixing of the polymer blend in the melt state may be expressed as[3,20]

$$f_{\text{mixing}} = \frac{\phi \ln \phi}{r_1} + \frac{(1-\phi)\ln(1-\phi)}{r_2} + \chi_{\text{FH}}\phi(1-\phi), \tag{3}$$

where $\phi_1=\phi$ and $\phi_2=(1-\phi)$ are the volume fractions of the crystalline component and the amorphous polymer (or solvent), respectively. r_1 and r_2 represent the number of the statistical segments or the lattice sites occupied by the constituents 1 and 2, respectively, whereas the amorphous-amorphous interaction is represented by $\chi_{\text{aa}}=\chi_{\text{FH}}=A+B/T$, where A and B are constants.[1,2] The phase field free energy of crystallization is described in terms of the Landau-type free energy expansion in the crystal order parameter, ψ,[20,21,26]

$$f_{\text{crystal}} = W\left[\frac{\psi^4}{4} - (\zeta+\zeta_0)\frac{\psi^3}{3} + \zeta\zeta_0\frac{\psi^2}{2}\right], \tag{4}$$

where W is the coefficient that represents the penalty for the nucleation process. ζ and ζ_0 represent the positions of the free energy maximum (i.e., unstable hump) and the solidification potential of crystallization (i.e., stable well) on the crystal order parameter axis, respectively.[20,21,26] Physically, the crystal order parameter (ψ) of a polymer crystal can be considered the ratio of the lamellar thickness (l) to the lamellar thickness of a perfect crystal (l^0), that is, $\psi=l/l^0$, and thus $\psi=0$ refers to the reference liquid (or melt) state, whereas $\psi=\zeta_0$ indicates the crystalline solid state.[16–21]

The free energy of the coupling interaction between the crystalline constituent and the amorphous component is given via the quadratic coupling, viz.,

$$f_{\text{coupling}} = \chi_{\text{ca}}\phi(1-\phi)\psi^2, \tag{5}$$

where χ_{ca} is the crystalline-amorphous interaction parameter, which is directly proportional to the heat of fusion, ΔH_u, but inversely proportional to the absolute temperature T, $\chi_{\text{ca}} \propto \Delta H_u/RT$.[20] The overall free energy of a blend containing a crystalline constituent becomes[20,21]

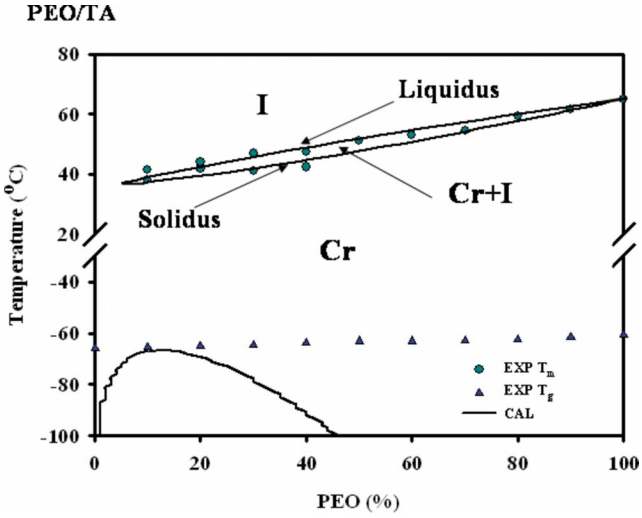

FIG. 3. (Color online) Comparison between the calculated self-consistent solutions (solid lines) and the experimental melting temperatures (filled circles) of PEO/TA blends showing the crystal solid-liquid coexistence region bound by the liquidus and solidus lines. The parameters used were ΔH_u=8.36 kJ/mol, χ_{aa}=0.0134, χ_{ca}=0.203 at 40 °C, r_1=110, r_2=2, and A=0 at T_{crit}=−260 °C. The predicted UCST falls below the glass transition temperatures of the blends.

$$f = \frac{\phi \ln \phi}{r_1} + \frac{(1-\phi)\ln(1-\phi)}{r_2} + \chi_{aa}\phi(1-\phi) + W\phi\left[\frac{\psi^4}{4} - (\zeta+\zeta_0)\frac{\psi^3}{3} + \zeta\zeta_0\frac{\psi^2}{2}\right] + \chi_{ca}\psi^2\phi(1-\phi). \tag{6}$$

The solid-liquid phase transition was determined first by minimizing the free energy with respect to the crystal order parameter, ψ,

$$\frac{\partial f}{\partial \psi} = W[\psi^2 - (\zeta+\zeta_0)\psi + \zeta\zeta_0] + 2\chi_{ca}(1-\phi) = 0. \tag{7}$$

The free energy penalty representing the solidification hump (barrier), W, is related to the heat of fusion, ΔH_u, as follows:[27]

$$W = \frac{6\Delta H_u}{RT}\left(1 - \frac{T}{T_m^0}\right)\left(\frac{1}{2} - \zeta\right)^{-1}, \tag{8}$$

where R is the gas constant and the terms in parentheses signify the correction for the supercooling effects. When the system approaches the equilibrium melting temperature, W is reduced to $W=6\Delta H_u/RT$, and thus it can be determined directly from the heat of fusion of the crystalline constituent. To determine the coexistent points, the equilibrium value of the crystal order parameter ψ thus obtained for each blend composition (ϕ) was subsequently substituted in the free energy expression, and then the pseudochemical potentials at each phase were balanced as follows:

$$\left.\frac{\partial f}{\partial \phi}\right|_{\phi^\alpha} = \left.\frac{\partial f}{\partial \phi}\right|_{\phi^\beta}. \tag{9}$$

The detailed procedures for seeking the self-consistent solution for the phase diagram pertaining to the double tangent method can be found elsewhere.[20,21]

Recently, an analytical expression was obtained by Rathi *et al.*[32] for the determination of the crystalline-amorphous interaction parameter from the experimental melting point depression data. Using the experimentally obtained χ_{ca} value, the validity of the present methodology was tested in comparison with the reported phase diagrams of the crystalline-amorphous polymer blends. Although the FH in-

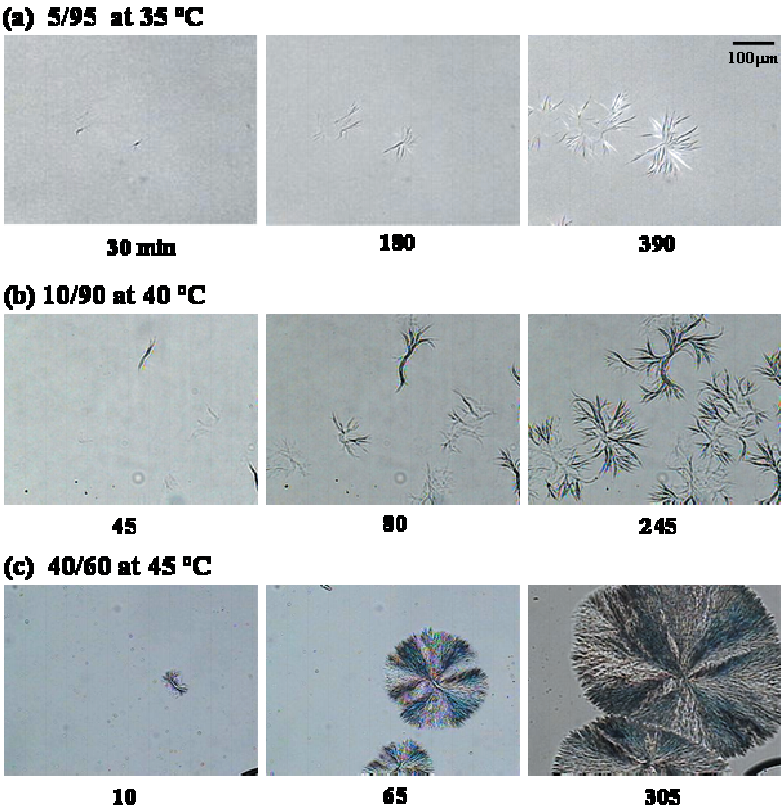

FIG. 4. (Color) Temporal emergence of the PEO crystals in the blend of the PEO/TA showing the coexistence of crystal+isotropic liquid: (a) the aggregates of anisotropic lamellar structure of PEO in the continuum of TA-rich melt in the 5/95 PEO/TA blend at 35 °C; (b) the sheaflike structure in the 10/90 blend at 40 °C; (c) the fully grown spherulite structure in the 40/60 blend at 45 °C.

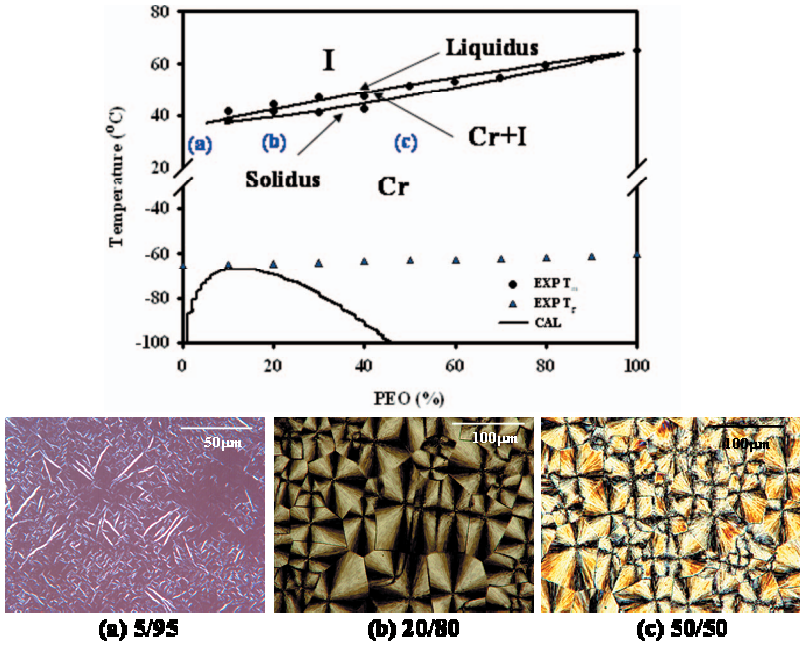

FIG. 5. (Color) Emerging PEO crystal structures following the isothermal crystallization by quenching various PEO/TA blends to 25 °C: (a) 5/95, (b) 20/80, and (c) 50/50, showing the solvated spherulites in conformity with the predicted single-phase crystalline region of the phase diagram.

teraction parameter controls the upper critical solution temperature (UCST), it plays a minor role in the determination of the melting point depression behavior. Contrary to the general perception, it is this crystal-amorphous interaction that has led to the lowering of the melting point.[32] Hence, it is important to distinguish the types of interactions, viz., liquid-liquid versus crystal solid-liquid interactions.

Figure 3 shows the self-consistent solution representing a solid-liquid coexistence gap bound by the solidus and liquidus lines. The parameters used were $\Delta H_u = 8.36$ kJ/mol, $\chi_{ca} = 0.203$, $\chi_{aa} = 0.0134$ at 40 °C, $r_1 = 110$ for PEO, $r_2 = 2$ for TA, and $A = 0$ at the critical temperature of $T_{crit} = -260$ °C. It is seen that the liquidus and solidus lines merged at a dilute concentration, exhibiting the crystal+liquid coexistence gap. In principle, the melting transition would drop asymptotically at the very dilute regime if the polymeric solvent is crystallizable or the UCST is close to the melting temperature of the constituent polymer. In the present case, there is no crystal melting temperature of TA, and the UCST is buried below the glass transition temperature, and thus the melting point disappeared abruptly at a very dilute concentration. Experimentally, there was no identifiable melting of PEO in the DSC runs at such low concentrations. Like the present calculation, the disappearance of the crystal melting in a crystalline polymer blend or solution is not unusual at least from the experimental point of view. For instance, poly(vinylidene fluoride) (PVDF) crystals completely disappeared when the poly(methyl methacrylate) (PMMA) concentration exceeded 60 wt %, and no melting transition was observed experimentally.[30] Although the close resemblance of the calculated solidus and liquidus lines to the experimental melting transition points is promising, it is important to confirm the phase morphology of each region.

Various temperature quenching experiments of three PEO/TA concentrations were conducted from the melt at

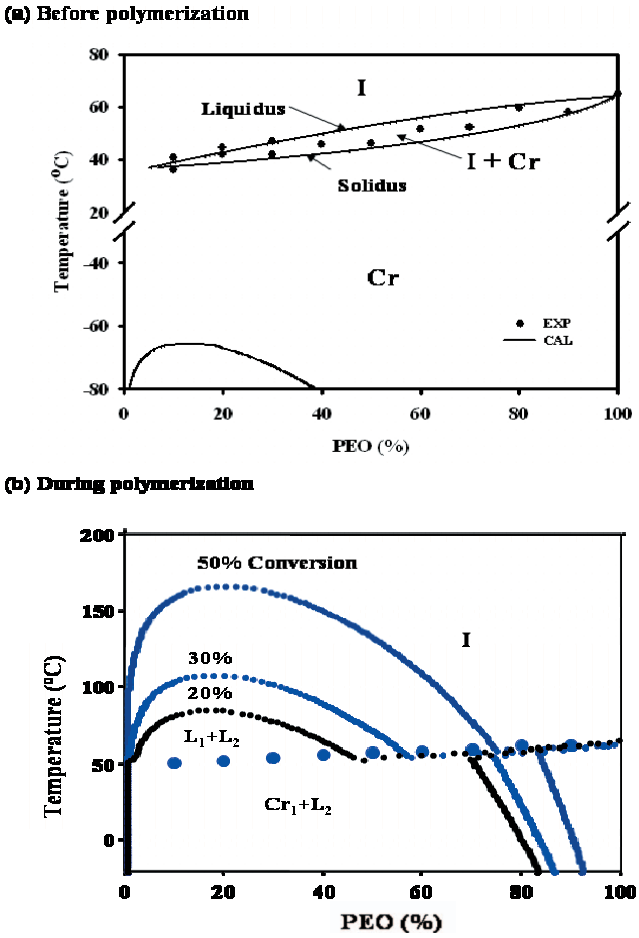

FIG. 6. (Color) Calculated snapshots of the coexistence curves evolving with reaction time in comparison with the experimental phase diagram of PEO/TA blend: (a) before and (b) during photopolymerization. With the progression of reaction, both the UCST and the melting transition curves move upward and surpass the reaction temperature, inducing phase separation and crystallization.

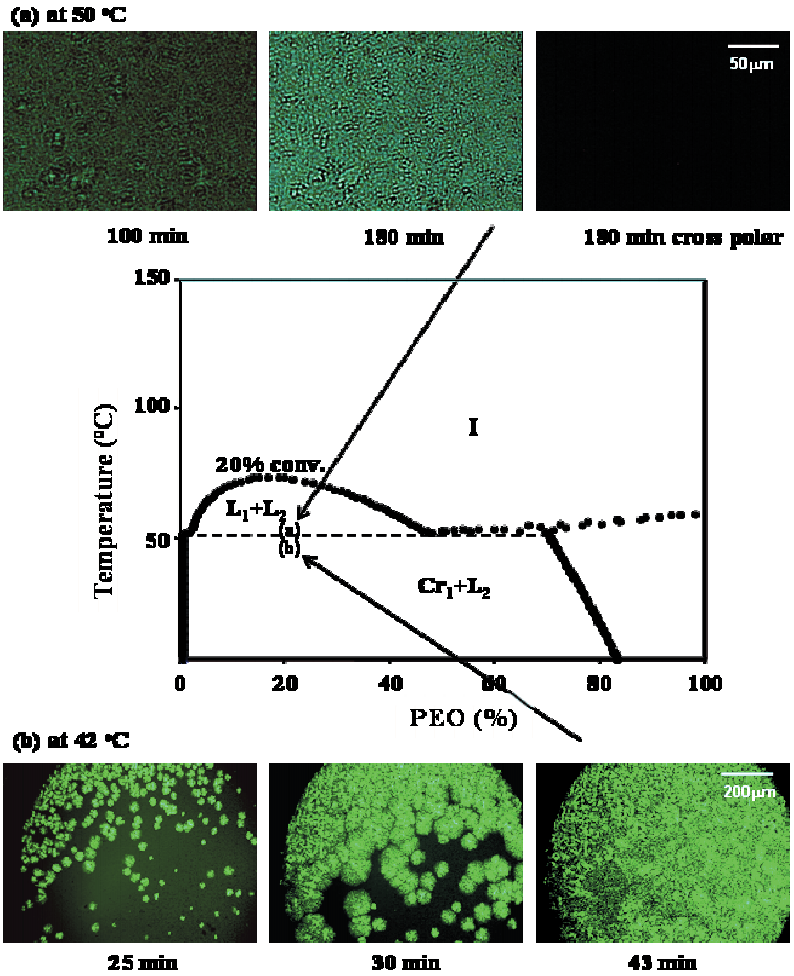

FIG. 7. (Color) Temporal evolution of phase morphology showing the liquid-liquid phase separation and crystallization during the course of photopolymerization of the 20/80 PEO/TA blends at (a) 50 °C and (b) 42 °C, respectively. The dark appearance under the crossed polarizers in Fig. 7(a) indicates the lack of orientation fluctuation (i.e., no crystalline order). The dashed line is the monotectic line representing the coexistence of liquid+liquid+solid phases at the 20% conversion, which virtually remains constant with further increase in the conversion.

80 °C to indicated temperatures corresponding to the solid-liquid coexistence gap. Figure 4(a) displays the temporal evolution of crystalline morphologies in the blend of 5/95 PEO/TA following temperature quench to 35 °C. Multiple nuclei reminiscent of lamellar single crystals develop in the early stage, which grow in size predominantly lengthwise. Subsequently, the primary lamellae branch out at both ends and then splay apart from each other. As a result of this continuous branching and splaying, these initial lamellae eventually evolve into open spherulitic structures or sheaflike textures; some of these nuclei show an anisotropic shape, especially in the 10/90 PEO/TA [Fig. 4(b)]. Likewise, the 20/80 PEO/TA mixture reveals a similar progression of the branched lamellar morphology or sheaflike crystals (picture not shown).

When the PEO concentration increases to 40%, the crystal structures evolve into a dense lamellar (or spherulitic) morphology. Regardless of the PEO crystal shapes at different compositions, all these crystal morphologies were found to coexist with the surrounding isotropic TA-rich liquid at the asymptotic equilibrium, thereby confirming the solid-liquid coexistence region.

Next, isothermal quenching was performed from the melt at 80 °C to a deeper temperature of 25 °C corresponding to the single-phase crystal region (Cr). Figure 5 shows the polarized optical micrographs of the emerging morphology of the 5/95, 20/80, and 50/50 PEO/TA blends. At the lower concentration of 5/95, numerous needlelike lamellae developed, which are presumably swollen in TA solvent. The unambiguous assignment of such opened lamellar structure to the single-phase crystal is difficult in the 5/95 PEO/TA blend because the amount of PEO materials is not sufficient to fill the whole microscopic view; this scenario may be more accurate at lower PEO concentrations, e.g., 1% or 2%. However, with increasing PEO content, the fully grown spherulites developed quickly and impinged onto each other, suggestive of the single-phase crystals. The observed hierarchical PEO crystal morphologies obtained at the asymptotic equilibrium are explicable by the Matkar–Kyu theory,[20] including the isotropic state, crystal+isotropic liquid, and single-phase crystalline regions of the crystalline-amorphous systems.

C. Photopolymerization-induced phase transitions

Figure 6(a) exhibits the comparison between the coexistence gap of the solid-liquid phase separation bound by the liquidus and solidus lines and the DSC melting temperatures of PEO in the PEO/TA/rose bengal blends containing other diluents such as cocuring agent and surfactant. The calculated UCST of the PEO/TA mixture was found to be located below the glass transition temperatures of the blends. The establishment of such a solid-liquid phase diagram is impor-

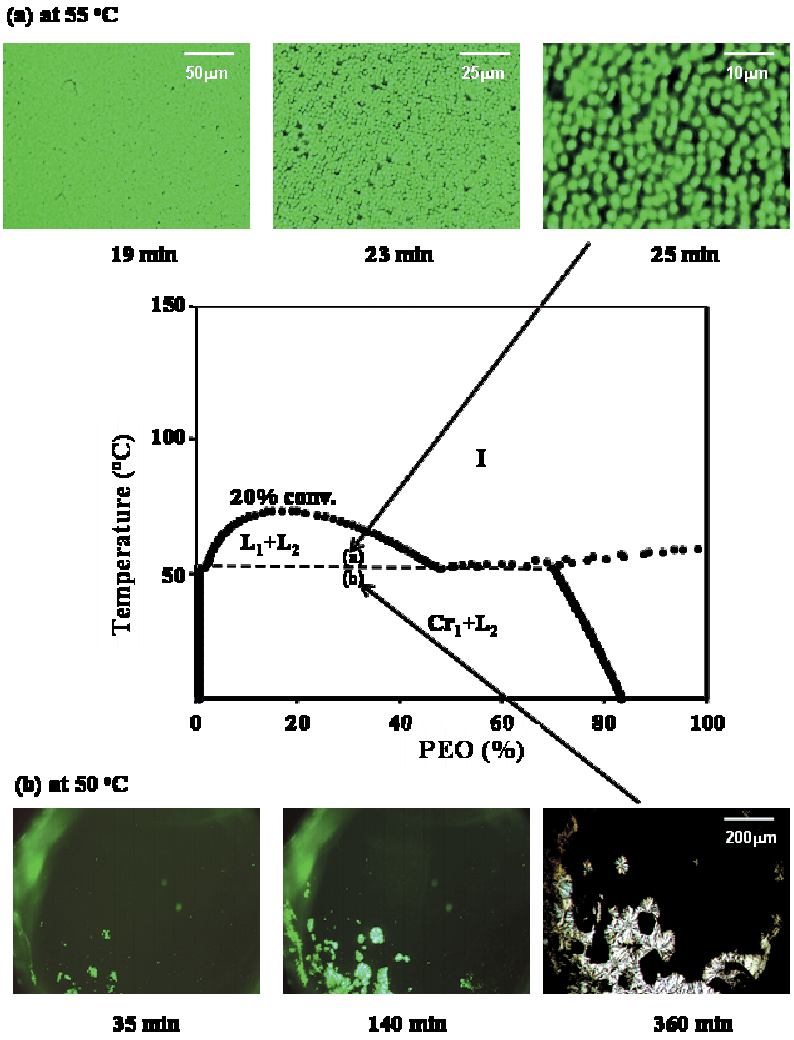

FIG. 8. (Color) (a) The liquid-liquid phase separation in the 30/70 PEO/TA blend driven by photopolymerization at 55 °C and (b) polymerization-induced crystallization at 50 °C, showing the epitaxial growth of PEO crystals.

tant as it provides guidance to the subsequent studies of photopolymerization-induced phase transitions.

When free radical polymerization is triggered via photoinitiation of rose bengal in the isotropic state, i.e., slightly above the depressed melting temperature, the molecular weight of TA increases followed by cross-linking. Figure 6(b) shows the calculated nonequilibrium snapshots of the UCST curves moving progressively with the extent of the reaction, protruding beyond the melting transition curve. Concurrently, the depressed melting curve moves upward in an attempt to restore back to the original melting temperature. At some conversions, say, 20%, the UCST as well as the solid-liquid transition line surpass the reaction temperature, which in turn drive the liquid-liquid phase separation as well as crystallization of the PEO constituent due to the photopolymerization of TA in the blends.

The development of the crystalline structure and phase morphology was investigated by performing the photopolymerization-induced phase transition at two different temperatures corresponding to point (a), which is at or slightly above the monotectic line, and to point (b), which is slightly below it (Fig. 7). Note that this monotectic line remains virtually unchanged with further increase in the conversion. The optical micrographs reveal the temporal emergence of (a) the phase separated domains of the 20/80 PEO/TA blend within the liquid-liquid region and (b) the dispersion of the PEO crystalline entities in the continuum of TA solvent. In the former, the emergence of the interconnected domains can be discerned under the unpolarized optical microscopic view, which is a signature of liquid-liquid phase separation probably occurring via spinodal decomposition (SD). Further, it shows a dark appearance under the polarized condition, suggesting that no orientation fluctuation develops, indicating the lack of crystalline structures. In the latter case of the photoreaction at point (b), multiple tiny spherulites develop, which grow in size with elapsed time. These spherulites coexist with the isotropic TA-rich melt.

A similar observation was made in another composition of the 30/70 blend. At 55 °C, i.e., above the monotectic line, denoted by (a) corresponding to the L_1+L_2 region, liquid-liquid phase separation takes place showing multiple droplets [Fig. 8(a)]. It should be cautioned that the observed droplets cannot be unambiguously assigned to the nucleation-growth mechanism. That is to say, the system first passes through the metastable gap before entering the unstable SD region where the SD would prevail; this mechanism is known as nucleation-assisted SD.[33] In the case of photopolymerization at 50 °C within the Cr_1+L_2 coexistence region, which is slightly below the monotectic line [Fig. 8(b)], epitaxial crys-

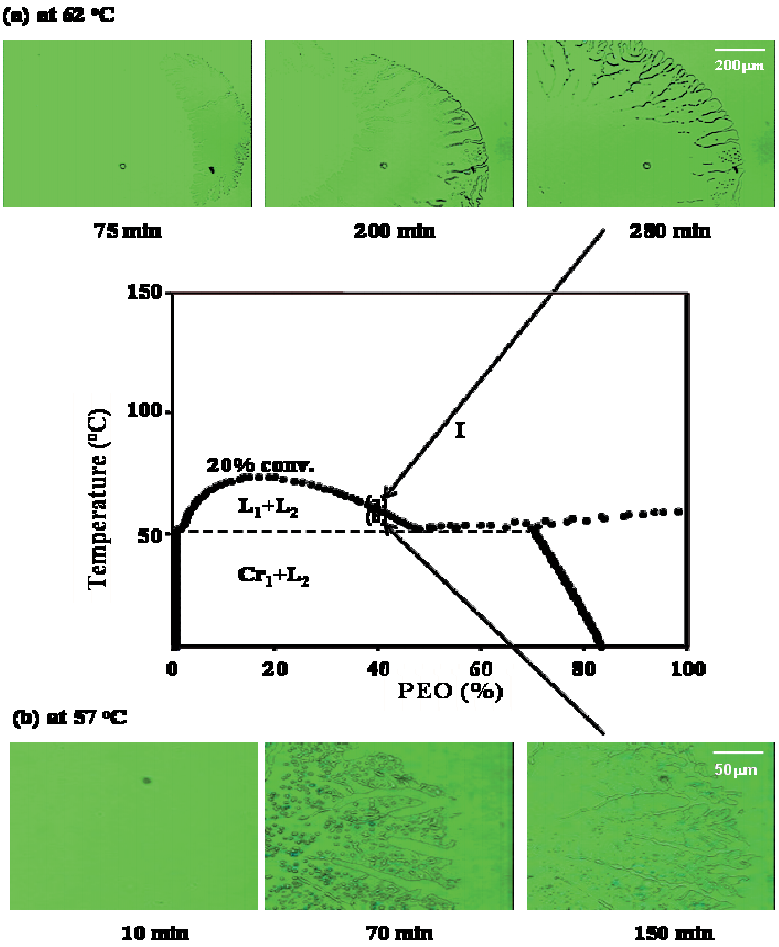

FIG. 9. (Color) Spatiotemporal evolution of the phase separated domains showing the fingerlike growth during photopolymerization of TA in the blends of 40/60 PEO/TA upon exposure at 17 $\mu W/cm^2$ of filtered green light, showing (a) phase separated domains within the viscous fingering pattern at 57 °C and (b) the regular viscous fingering without any phase separated texture at 62 °C.

tal growth occurs from the circumference of the illuminated beam, which may be driven by the photointensity gradient at the peripheral.

In the case of photopolymerization of the 40/60 PEO/TA blends at 50 °C, the viscous fingering takes place while the phase separated droplets were formed within these propagating viscous fingering patterns [Fig. 9(b)]. When the polymerization reaction temperature was further raised above the monotectic line to 55 °C, the viscous fingering starts at the peripheral, and it propagates with elapsed reaction time toward the middle by branching and tip splitting. This viscous fingering process may be attributed to the viscosity mismatch between the PEO melt and the network-forming TA fluid. Of particular interest is the occurrence of liquid-liquid phase separation within these viscous fingering patterns. These phase separated domains tend to diminish with further progression of reaction time. However, such phase separated domains are found to be absent in the case of polymerization at a higher temperature of 62 °C [Fig. 9(a)]. This temperature accidentally corresponds to the isotropic region, i.e., above the liquid-liquid coexistence curve of the 20% conversion and thus the phase separated structures if any would have been homogenized. This conjecture may be valid only if the reaction is very slow. With continued reaction, liquid-liquid phase separation is anticipated to occur.

IV. CONCLUSIONS

We have demonstrated that PEO and TA are miscible in the amorphous state although they may not achieve a complete miscibility due to the presence of PEO crystals in the PEO/TA blends. The observed dual melting peaks in lower PEO compositions can be attributed to the Cr+I coexistence region bound by the liquidus and solidus coexistence lines. The self-consistent solution of the combined FH demixing theory and the phase field theory of solidification was found to accord well the experimental phase diagrams of the present PEO/TA system. The coexistence regions are further confirmed by the emerging phase morphology following the thermal quenches into each region. Moreover, it was found that the blend morphology depends on the competition between photopolymerization-induced crystallization and liquid-liquid phase separation in a manner dependent on the PEO/TA blend compositions and reaction temperatures. It is reasonable to imply that the emerging morphologies depend on the pathway across the phase boundaries traversed by the system.

ACKNOWLEDGMENTS

Support of this work by the National Science Foundation through Grant No. DMR 0514942 is gratefully acknowledged.

[1] D. R. Paul and S. Newman, *Polymer Blends* (Academic, New York, 1978), Vols. I–II.
[2] O. Olabisi, L. M. Robeson, and M. T. Shaw, *Polymer-Polymer Miscibility* (Academic, New York, 1979).
[3] P. J. Flory, *Principles of Polymer Chemistry* (Cornell University Press, New York, 1953).
[4] P. H. Geil, *Polymer Single Crystals* (Interscience, New York, 1963).

[5] H. Tanaka and T. Nishi, Phys. Rev. Lett. **55**, 1102 (1985).
[6] H. Tanaka and T. Nishi, Phys. Rev. A **39**, 783 (1989).
[7] M. Avella, E. Martuscelli, and P. Greco, Polymer **32**, 1647 (1991).
[8] M. Avella, E. Martuscelli, and M. Raimo, Polymer **34**, 3234 (1993).
[9] J. P. Penning and R. St. J. Manley, Macromolecules **29**, 84 (1996).
[10] K. Fujita, T. Kyu, and R. St. J. Manley, Macromolecules **29**, 91 (1996).
[11] C. Daniel, A. Menelle, A. Brulet, and J. M. Guenet, Polymer **38**, 4193 (1997).
[12] B. Ray, S. Elhasri, A. Thierry, P. Marie, and J. M. Guenet, Macromolecules **35**, 9730 (2002).
[13] T. Ikehara and T. Nishi, Polym. J. (Tokyo, Jpn.) **32**, 683 (2000).
[14] Z. Qiu, T. Ikehara, and T. Nishi, Polymer **44**, 2799 (2003).
[15] F. Drolet, K. R. Elder, M. Grant, and J. M. Kosterlitz, Phys. Rev. E **61**, 6705 (2000).
[16] T. Kyu, R. Mehta, and H.-W. Chiu, Phys. Rev. E **61**, 4161 (2000).
[17] R. Mehta, W. Keawwattana, A. L. Guenthner, and T. Kyu, Phys. Rev. E **69**, 061802 (2004).
[18] H. Xu, R. Matkar, and T. Kyu, Phys. Rev. E **72**, 011804 (2005).
[19] S. J. Park, P. Rathi, and T. Kyu, Phys. Rev. E **75**, 051804 (2007).
[20] R. A. Matkar and T. Kyu, J. Phys. Chem. B **110**, 12728 (2006).
[21] R. A. Matkar and T. Kyu, J. Phys. Chem. B **110**, 16059 (2006).
[22] A. Matsuyama, J. Phys. Soc. Jpn. **75**, 034604 (2006).
[23] S.-K. Chan, J. Chem. Phys. **67**, 5755 (1977).
[24] P. R. Harrowell and D. W. Oxtoby, J. Chem. Phys. **86**, 2932 (1987).
[25] A. A. Wheeler, W. J. Boettinger, and G. B. McFadden, Phys. Rev. A **45**, 7424 (1992).
[26] R. Kobayashi, Physica D **63**, 410 (1993).
[27] O. Valdes-Aguilera, C. P. Pathak, J. Shi, D. Watson, and D. C. Neckers, Macromolecules **25**, 541 (1992).
[28] T. J. Bunning, L. V. Natarajan, V. P. Tondiglia, and R. L. Sutherland, Annu. Rev. Mater. Sci. **30**, 83 (2000).
[29] H. Duran, S. Meng, N. Kim, J. Hu, T. Kyu, L. V. Natarajan, V. P. Tondiglia, and T. J. Bunning, Polymer **49**, 534 (2008).
[30] T. Nishi and T. T. Wang, Macromolecules **8**, 909 (1975).
[31] P. Smith and R. St. J. Manley, Macromolecules **12**, 483 (1979).
[32] P. Rathi, T.-M. Huang, P. Dayal, and T. Kyu, J. Phys. Chem. B **112**, 6460 (2008).
[33] T. Kyu and J. H. Lee, Phys. Rev. Lett. **76**, 3746 (1996).